Proceedings of GT2005
ASME Turbo Expo 2005: Power for Land, Sea and Air
June 6-9, 2005, Reno-Tahoe, Nevada, USA

GT2005-68382

Catalytic Combustion Systems for Micro-Scale Gas Turbine Engines

C. M. Spadaccini*, J. Peck, and I. A. Waitz
Gas Turbine Laboratory
Department of Aeronautics and Astronautics
Massachusetts Institute of Technology
Cambridge, MA 02139

ABSTRACT

As part of an ongoing effort to develop a micro-scale gas turbine engine for power generation and micropropulsion applications, this paper presents the design, modeling, and experimental assessment of a catalytic combustion system. Previous work has indicated that homogenous gas-phase microcombustors are severely limited by chemical reaction time-scales. Storable hydrocarbon fuels, such as propane, have been shown to blowout well below the desired mass flow rate per unit volume. Heterogeneous catalytic combustion has been identified as a possible improvement. Surface catalysis can increase hydrocarbon-air reaction rates, improve ignition characteristics, and broaden stability limits. Several radial inflow combustors were micromachined from silicon wafers using Deep Reactive Ion Etching (DRIE) and aligned fusion wafer bonding. The 191 mm^3 combustion chambers were filled with platinum coated foam materials of various porosity and surface area. For near stoichiometric propane-air mixtures, exit gas temperatures of 1100 K were achieved at mass flow rates in excess of 0.35 g/s. This corresponds to a power density of approximately 1200 MW/m^3; an 8.5-fold increase over the maximum power density achieved for gas-phase propane-air combustion in a similar geometry. Low order models including time-scale analyses and a one-dimensional steady-state plug-flow reactor model, were developed to elucidate the underlying physics and to identify important design parameters. High power density catalytic microcombustors were found to be limited by the diffusion of fuel species to the active surface, while substrate porosity and surface area-to-volume ratio were the dominant design variables.

NOMENCLATURE

A	Arrhenius pre-exponential factor
a,b	Arrhenius exponents
a_v	surface area-to-volume ratio
d_h	hydraulic diameter
C_b	molar concentration
C_p	constant pressure specific heat
D	diffusion coefficient
Da_1	residence time-based Damköhler number
Da_2	diffusion-based Damköhler number
E″	heat loss
E	heat generated
E_a	activation energy
h	enthalpy or heat transfer coefficient
j_D	j-factor for mass transport
j_H	j-factor for heat transfer
k_m	mass transport coefficient
k	reaction rate constant
l	length scale
LHV	lower heating value
M	molecular weight
$\dot{m}$	mass flow
P	pressure
Pe	Peclet number
Pr	Prandtl number
$\dot{Q}_{loss}$	heat loss from combustor
R	gas constant
(-R)	reaction rate
Re	Reynolds number
Sc	Schmidt number

* current address
Center for Micro and Nano Technology
Lawrence Livermore National Laboratory
P.O. Box 808, L-223
7000 East Avenue
Livermore, CA 94551
(925)423-3185
spadaccini2@llnl.gov

S_f	shape factor
T	temperature
V	volume
v	velocity or diffusion volume
w	thickness
Y	mole fraction
z	axial location
η_c	overall combustor efficiency
$\eta_{chemical}$	chemical efficiency
$\eta_{thermal}$	thermal efficiency
ρ	fluid density
$\tau_{diffusion}$	diffusion time
$\tau_{reaction}$	reaction time
$\tau_{residence}$	residence time

Subscripts

A,B	species
a	air
b	bulk
f	fuel
s	surface
0	initial condition
1	combustor inlet
2	combustor exit

1. INTRODUCTION

Advances in silicon microfabrication techniques and microelectromechanical systems (MEMS) have led to the possibility of a new generation of micro heat engines for power generation and micro air-vehicle propulsion applications. Epstein *et al.* [1] and Groshenry [2] have reported the design for a silicon-based, micro gas turbine generator that may be capable of producing 10-50 Watts of power in a volume less than 1 cm^3 while consuming 7 grams of fuel per hour. Like their larger counterparts, an engine of the type shown in Figure 1 requires a high temperature combustion system to convert chemical energy into fluid thermal and kinetic energy.

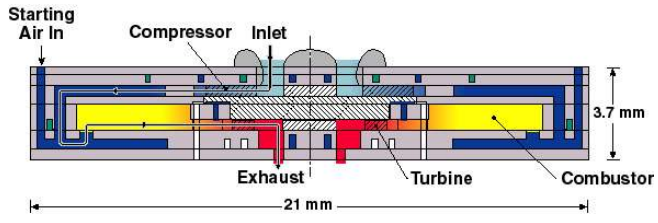

Figure 1. Baseline engine schematic.

Previous work in this area has shown that homogenous gas-phase microcombustors are limited by chemical reaction time-scales [3,4,5]. Although hydrogen-air mixtures have been successfully burned in small volumes for micro gas turbine applications, storable hydrocarbon fuels, such as propane, will not combust at the desired mass flow rates within the desired combustor volumes [5]. As result, heterogeneous catalytic processes have been pursued to increase reaction rates and improve stability.

This paper presents the results of work toward achieving high power density (high mass flow rate) operation of a microcombustion system with propane-air mixtures. These studies have resulted in the identification of critical design trades and recommendations for microcombustor design.

Section 2 discusses the challenges of combustion in a micro-scale environment and overviews previous work towards the development of silicon-based systems. The design, materials, and testing methodology for catalytic microcombustors are introduced in Section 3. In Section 4, results from testing of these devices are presented and Section 5 includes a low-order modeling effort to explain performance trends. Section 6 reviews design recommendations and trade-offs while Section 7 summarizes the paper and presents areas of future work.

2.0 MICROCOMBUSTION CHALLENGES

The functional requirements of a microcombustor are similar to those of a conventional gas turbine combustor. These include the efficient conversion of chemical energy to fluid thermal and kinetic energy with low total pressure loss, reliable ignition, and wide flammability limits. However, the obstacles to satisfying these requirements are different for a micro-scale device. As first described by Waitz *et al*. [6], a micro-scale combustor is more highly constrained by inadequate residence time for complete combustion and high rates of heat transfer from the combustor. Microcombustor development also faces unique challenges due to material and thermodynamic cycle constraints. These constraints are reviewed in the following sections.

2.1 TIME-SCALE CONSTRAINTS

For the energy conversion applications we are interested in, power density is the most important metric. As shown in Table 1, the high power density of a microcombustor directly results from high mass flow per unit volume. Since chemical reaction times do not scale with mass flow rate or combustor volume, the realization of this high power density is contingent upon completing the combustion process within a shorter combustor through-flow time.

For gas-phase combustors, this fundamental time constraint can be quantified in terms of a residence time-based Damköhler number; the ratio of the residence time to the characteristic chemical reaction time.

$$Da_1 = \frac{\tau_{residence}}{\tau_{reaction}} \quad (1)$$

Table 1: A comparison of the operating parameters and requirements for a microengine combustor with those estimated for a conventional GE90 combustor. (Note: residence times are calculated using inlet pressure and an average flow temperature of 1000 K.)

	Conventional Combustor	Microcombustor
Length	0.2 m	0.001 m
Volume	0.073 m^3	6.6×10^{-8} m^3
Cross-sectional area	0.36 m^2	6×10^{-5} m^2
Inlet total pressure	37.5 atm	4 atm
Inlet total temperature	870 K	500 K
Mass flow rate	140 kg/s	1.8×10^{-4} kg/s
Residence time	~7 ms	~0.5 ms
Efficiency	>99%	>90%
Pressure ratio	>0.95	>0.95
Exit temperature	1800 K	1600 K
Power Density	1960 MW/m^3	3000 MW/m^3

To ensure a Da_1 greater than unity (and complete combustion), a designer of a microcombustor can either increase the flow residence time or decrease the chemical reaction time. The characteristic combustor residence time is given by the bulk flow through the combustor volume.

$$\tau_{residence} \approx \frac{\text{volume}}{\text{volumetric flow rate}} = \frac{VP}{\dot{m}RT} \tag{2}$$

Residence time can be increased by increasing the size of the chamber, reducing the mass flow rate, or increasing the operating pressure. A chemical reaction time can be approximated by an Arrhenius type expression.

$$\tau_{reaction} \approx \frac{[fuel]_0}{A[fuel]^a[O_2]^b e^{-E_a/RT_0}} \tag{3}$$

Reaction time is primarily a function of fuel properties and the mixture temperature and pressure.

Since high power density requirements mandate high mass flow rates through small chamber volumes, the mass flow rate per unit volume can not be reduced without compromising device power density. Hence, there is a basic tradeoff between power density and flow residence time.

$$\text{Power density} \propto \frac{\dot{m}}{V} \propto \frac{\dot{m}_f LHV}{V} \propto \frac{\rho}{\tau_{residence}} \tag{4}$$

For a given operating pressure (and thus density), and assuming a fixed Da_1, reducing the chemical reaction time and thus required residence time, is the only means of ensuring complete combustion without compromising the high power density of the device.

One means of reducing this chemical reaction time-scale is to utilize heterogeneous surface catalysis. This oxidation process is fundamentally different than that occurring in a gas-phase combustion system. Typically, the reactions are significantly faster and there is no flame structure since the chemistry takes place on the catalyst surface. However, use of surface reactions introduces an additional time-scale to consider when determining the rate controlling process. The diffusion of the reactant species to the catalyst surface is often the controlling phenomenon. This diffusion time is related to the molecular diffusion coefficient for one species being transported through another and can be estimated using the Fuller correlation [7]

$$D_{AB} = \frac{1.013 \times 10^{-2} T^{1.75} \left(\frac{1}{M_A} + \frac{1}{M_B} \right)^{1/2}}{P\left[\left(\sum v_i \right)_A^{1/3} + \left(\sum v_i \right)_B^{1/3} \right]^2}. \tag{5}$$

Noting that the diffusion time can be a critical factor in these systems, two additional non-dimensional parameters become relevant. The diffusion-based Damköhler number can be written as the ratio of the diffusion time to the characteristic chemical reaction time

$$Da_2 = \frac{\tau_{diffusion}}{\tau_{reaction}} = \frac{(-R)d_h}{C_{b,s} D_{A,B}} \tag{6}$$

and indicates whether chemistry or mass transport are dominant. The Peclet number is defined as the ratio of the diffusion time to the residence time

$$Pe = \frac{\tau_{diffusion}}{\tau_{residence}} = \frac{v_b d_h}{D_{A,B}}. \tag{7}$$

Peclet numbers larger than unity imply that significant quantities of reactants are being passed through the combustor without reaching the catalyst surface and reacting. For a high power density microcombustor with short through-flow times, this is the most fundamental limitation on power density.

2.2 HEAT TRANSFER EFFECTS AND FLUID-STRUCTURE COUPLING

Energy loss due to heat transfer at the walls of the combustion chamber in a conventional gas turbine is typically neglected. However, for a microcombustor this is an important factor. The surface area-to-volume ratio for a micro-scale combustor is approximately 500 m^{-1}, or two orders of magnitude larger than that of a typical combustor.

Waitz *et al*. [6] have shown that the ratio of heat lost to that generated scales with the hydraulic diameter as follows:

$$\frac{E''}{\dot{E}} \propto \frac{1}{d_h^{1.2}}. \quad (8)$$

The hydraulic diameter of a microcombustor is on the order of millimeters, hundreds of times smaller than that of a typical combustor. Therefore, the ratio of heat lost to that generated may be as much as two orders of magnitude greater than that of a large-scale combustor.

The effect of this large surface heat loss on homogeneous gas-phase combustion is twofold. First, large thermal losses have a direct impact on overall combustor efficiency. Therefore, typical large-scale combustor efficiencies of greater than 99% are not feasible. Second, heat loss can increase kinetic times and narrow flammability limits through lowering reaction temperatures. This can exacerbate the constraints of short residence time.

In addition, the structures fabricated for these microcombustors are etched from silicon which has a high thermal conductivity. This combined with the short heat conduction paths at the micro-scale lead to Biot numbers much less than unity (of order 0.01) and structures that tend to be isothermal. These heat transfer issues have a significant impact on catalytic systems where the heat is generated on a surface. The heat generated is more likely to be conducted away through the structure than transferred through a thermal boundary layer to the bulk flow. This can further reduce power density.

2.3 MATERIAL CONSTRAINTS

There are also several material constraints imposed upon a silicon microcombustion system. The most critical requirement is a wall temperature limit of less than ~1300 K. At temperatures above this level, silicon begins to soften and lose its structural integrity. However, high surface heat transfer and the high thermal conductivity of silicon are beneficial in this case. Combustor wall temperatures can be kept below the 1300 K requirement by conduction of heat through the structure to the ambient. In addition, the rotating components of the microengine must maintain even lower wall temperatures, below 1000 K, due to creep considerations.

There are further material constraints imposed upon the system when utilizing thin films of noble metal catalysts. Typically platinum-based, these materials will begin to agglomerate when exposed to temperatures in excess of ~1200 K for significant periods of time. This will reduce the active surface area on which catalysis can occur.

2.4 PREVIOUS WORK

Mehra and Waitz [8] were the first to develop a silicon, microfabricated combustor compatible with a realistic engine geometry. This combustor was 0.066 cm^3 in volume and was designed to operate using lean, premixed, hydrogen-air combustion. It was tested over a range of equivalence ratios spanning from 0.4 to 1.6 for a fixed mass flow rate of 0.045 g/s and atmospheric pressure. For premixed hydrogen-air operation, exit gas temperatures in excess of 1800 K were achieved with combustor efficiencies up to 70% and power densities near 1200 MW/m^3.

A more substantial six silicon wafer combustor, shown in Figure 2, was also designed and tested by Mehra [3,4]. This device consisted of a 191 mm^3 volume and a wrap-around thermal isolation jacket. For gas phase hydrogen-air operation, exit gas temperatures in excess of 1800 K and efficiencies near 100% were achieved at mass flow rates of 0.12 g/s. This corresponds to a power density over 1100 MW/m^3. However, this device did not achieve the target mass flow rate of 0.36 g/s due residence time constraints resulting in flame blowout around 0.20 g/s.

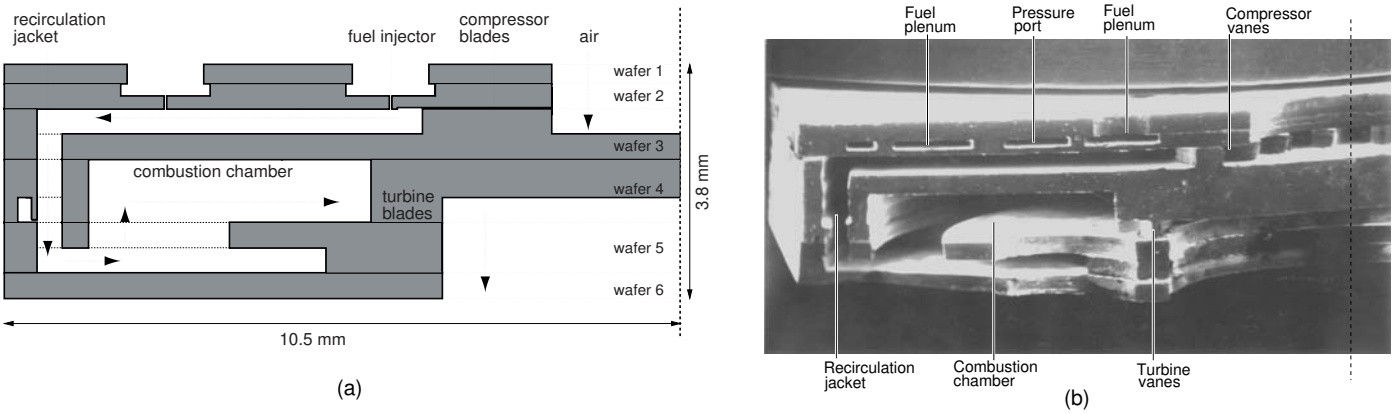

Figure 2. Schematic (a) and SEM (b) of six-wafer microcombustor.

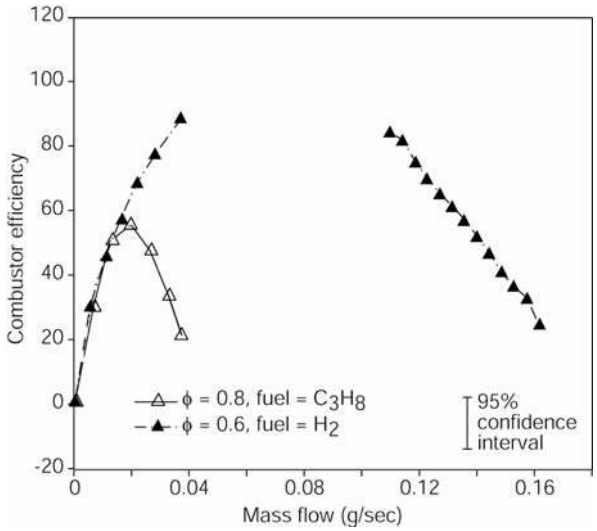

Figure 3. Comparison of hydrogen and propane gas-phase performance.

Spadaccini [5,9] improved upon the gas-phase performance of the device by converting it to a dual-zone operating mode similar to that found in conventional-scale combustors. This consisted of a hot primary-zone followed by a dilution-zone. This was achieved by etching a series of holes through the upper wall of the combustion chamber splitting the flow in the thermal isolation jacket. Approximately half of the flow entered the combustor and burned near stoichiometric conditions in the primary-zone while the other half entered through the top wall of the chamber to dilute and cool the flow to the appropriate exit temperature. The stable, hot primary-zone increased reaction rates and improved performance allowing operation above 0.22 g/s. However, this was still short of the design mass flow rate.

Spadaccini *et. al.* [5] also tested several hydrocarbon fuels, including propane and ethylene in the six-wafer combustors. The ~5-20 times slower reaction rates of these fuels exacerbated the residence time constraints. This resulted in maximum mass flow rates of ~0.07 g/s and power densities less than 300 MW/m^3, well below the targets for micro gas turbine engine operation. Figure 3 highlights the performance difference between hydrogen and propane fuel. Furthermore, it has been the long term goal of much of this work to achieve high power density operation of a microcombustor using storable hydrocarbon fuels. For this reason, propane-air combustors utilizing heterogeneous surface catalysis have been pursued and are the subject of the remainder of this paper.

There are several research groups pursuing microcombustors for other types of small scale power sources. Typically, these combustors run at significantly lower mass flow rates and power densities. This includes a silicon micromachined rotary engine being developed at the University of California, Berkeley which involves combustion of gas-phase hydrogen-air mixtures ignited with a spark or glow-plug [10]. Other catalytic microcombustor work has been conducted at MIT for suspended tube microreactors [11] and for thermoelectric generators [12]. A "*swiss-roll*" catalytic microcombustor has been developed at the University of Southern California for use as a thermoelectric generator with recuperation [13] while the smallest known combustor was fabricated and tested at the University of Oregon and burns propane catalytically over a platinum wire [14] in a volume of 0.050mm^3.

3.0 EXPERIMENTAL APPROACH

To improve upon previous propane-air performance in the baseline six-wafer combustors, heterogeneous surface catalysis was implemented. For the experiments presented here, the baseline six-wafer device was used as the test device and platinum was chosen as the catalyst material.

3.1 SIX-WAFER CATALYTIC MICROCOMBUSTOR

The baseline six-wafer device which had been used for previous experiments was fitted with platinum coated foam materials. Figure 4 indicates the location of the catalyst material inside the device. The silicon was etched using Deep Reactive Ion Etching (DRIE) and the wafers were aligned and fusion bonded together. The details of these microfabrication steps can be reviewed in references [3] and [4]. The process of implanting the platinum coated foam material into the devices during fabrication is discussed in [9] and [15]. The substrate materials and platinum deposition are presented in the following sections.

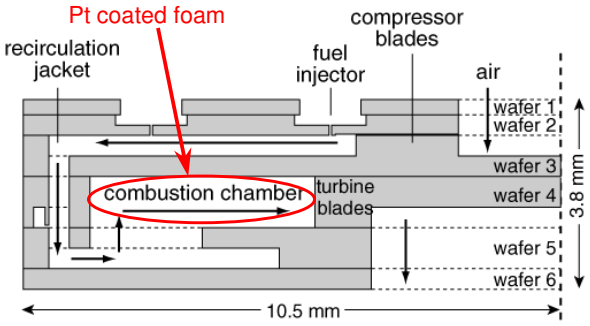

Figure 4. Schematic of microcombustor showing location of catalyst material.

3.2 CATALYST SUBSTRATE MATERIALS

Several catalyst substrate materials were used. This included a nickel foam material with a porosity of approximately 95%, a FeCrAlY foam with a porosity of 88.5%, and an Inconel-625 foam which was 78% porous. Porosity is defined as the ratio of open volume to total volume of the material. This parameter will be referred to as α and can be written as

$$\alpha = \frac{V_{open}}{V_{total}}. \quad (9)$$

The foam substrate materials are shown in Figures 5, 6, and 7 where items a and b are photographs and SEMs respectively.

3.3 CATALYST MATERIALS

After machining to the size and shape of the combustion chamber, the foam substrates required a platinum coating. Two methods were utilized to produce these layers. The first involved dipping the substrate in a chloroplatinic acid solution while the second consisted of using ionic plasma deposition. The first technique was performed on the 95% porous nickel substrate and the second technique on the FeCrAlY and Inconel-625.

Unsupported metal catalysts can be deposited onto a substrate using a solution of metal salt. In this procedure, the metal salt (H_2PtCl_6 in this case) is dissolved in deionized water. The substrate pieces are soaked in this solution then placed in a small tube furnace. The water is then evaporated followed by reacting the remaining compound with hydrogen at elevated temperature to remove the Cl in the form of HCl leaving only platinum on the surface. The nickel foam pieces were coated using this technique and typically increased in weight by approximately 3%-5% creating layers approximately 2-3 μm thick. The procedure used is described in reference [9].

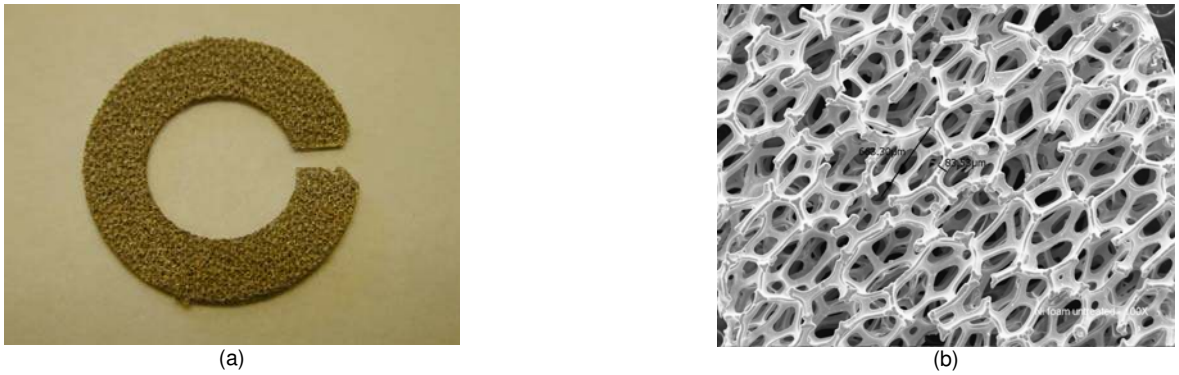

(a) (b)

Figure 5. Photograph (a) and SEM (b) of 95% porous nickel foam substrate.

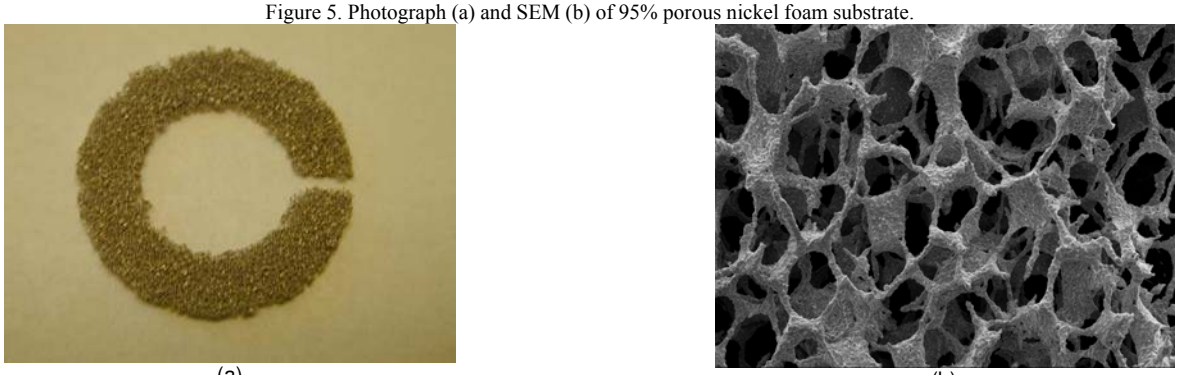

(a) (b)

Figure 6. Photograph (a) and SEM (b) of 88.5% porous FeCrAlY foam substrate.

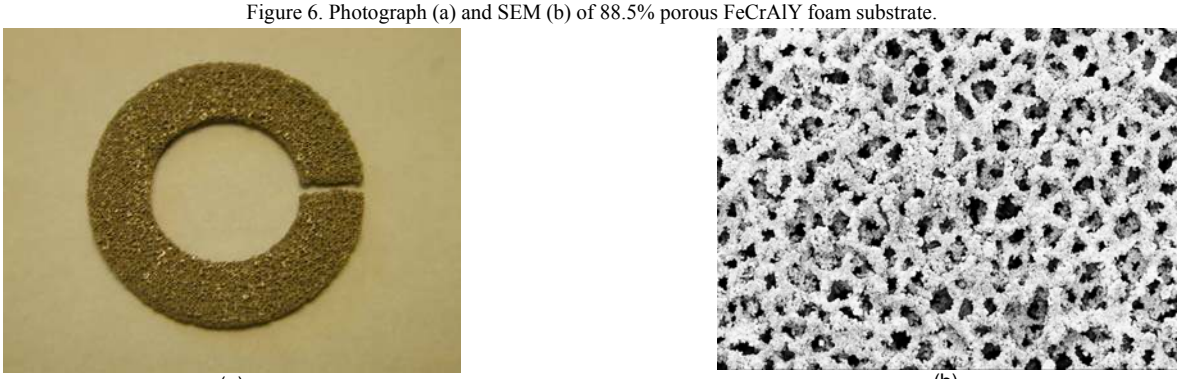

(a) (b)

Figure 7. Photograph (a) and SEM (b) of 78% porous Inconel-625 foam substrate.

The FeCrAlY and Inconel-625 substrates were coated using ionic plasma deposition. This is a proprietary process developed by Ionic Fusion Corporation and involves propelling atoms of a given material by ionic acceleration and ballistically impregnating a substrate. It is a high energy, low temperature process that provides good penetration into porous substances [16]. The foam pieces were first coated with 2-3 μm of either Al_2O_3 or ZrO_2 followed by 2-3 μm of platinum. The FeCrAlY and Inconel-625 pieces increased in weight by approximately 4% and 2% respectively. The ceramic inter-layers acted as a diffusion barrier between the platinum and the metal substrates and are discussed in more detail in reference [9].

3.4 EXPERIMENTAL SETUP AND DIAGNOSTICS

Prior to testing, the microcombustors were packaged into a suitable test rig. In order to connect the device's micro-scale fluid channels to a macro-scale feed system, a glass bead interconnect scheme was developed by Mehra [3]. Small kovar tubing was hermetically sealed to the silicon with glass beads and brazed to a larger metal plate for connection to conventional fittings. A fully packaged device is shown in Figure 8. A more detailed description of this process can be found in references [3], [17], and [18].

Due to the micro-scale of the devices, it is difficult to obtain non-intrusive measurements. Therefore, diagnostics were limited. Exit gas temperature was measured using a 0.010" sheathed type K thermocouple. Because of the large temperature gradients along the length of the wire, an error analysis for the thermal conductivity, radiative emissivity, and calibration drifts predicted uncertainties up to ±130 K. A wall temperature measurement was also obtained with the same type thermocouple and an uncertainty of ±12 K. In addition to the temperature diagnostics, pressure was measured upstream in the cooling jacket and in the combustion chamber itself. A detailed uncertainty analysis can be found in reference [3].

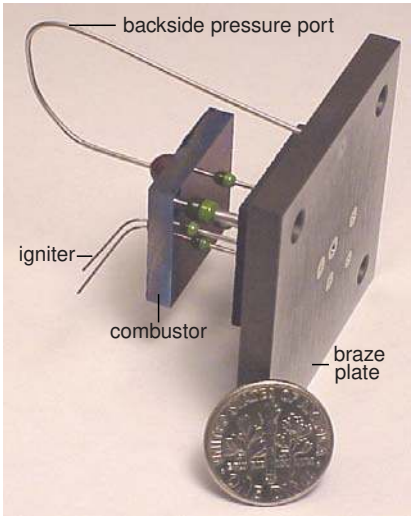

Figure 8. Fully packaged microcombustor.

4.0 EXPERIMENTAL RESULTS

Overall combustor efficiency is defined as:

$$\eta_c = \frac{(\dot{m}_a + \dot{m}_f)h_2 - \dot{m}_a h_1}{\dot{m}_f h_f} \tag{10}$$

where station (1) refers to the combustor inlet and station (2) is the combustor exit. The combustor efficiency can be written as the product of a *chemical efficiency*, and a *thermal efficiency*. These two efficiencies can be written as:

$$\eta_{chem} = \frac{[(\dot{m}_a + \dot{m}_f)h_2 - \dot{m}_a h_1] + \dot{Q}_{loss}}{\dot{m}_f h_f} = \frac{\text{total enthalpy released}}{\text{maximum enthalpy release possible}} \tag{11}$$

$$\eta_{therm} = \frac{(\dot{m}_a + \dot{m}_f)h_2 - \dot{m}_a h_1}{[(\dot{m}_a + \dot{m}_f)h_2 - \dot{m}_a h_1] + \dot{Q}_{loss}} = \frac{\text{enthalpy rise of fluid}}{\text{total enthalpy released}} \tag{12}$$

4.1 IGNITION CHARACTERISTICS

To ignite, the catalyst had to be heated using an external radiant heater to a suitable ignition temperature. Upon reaching this temperature, a hydrogen-air mixture was passed through the device and over the platinum catalyst. Initiation of the surface reaction ensued and both the wall and gas temperatures rose to a steady-state value. To accomplish this in the microcombustors, the entire chip was preheated with an external heater [19]. After achieving ignition, the heater was removed and the device continued to operate via autothermal combustion of the hydrogen-air mixture over platinum. Typically, a catalytic combustor will exhibit an ignition/extinction hysteresis similar to that shown by Schmidt *et al.* [20,21]. For the 95% porous nickel foam and the 88.5% porous FeCrAlY foam this is shown in Figure 9. Wall temperature is plotted against heater power and ignition occurs at a heater power of approximately 20%-30% (around 80-100°C). This figure is intended only to qualitatively show the ignition process and to illustrate the hysteresis.

Although the catalytic microcombustors initially ignite with a hydrogen-air mixture, ultimately, the goal is to achieve autothermal combustion of propane-air mixtures over the platinum catalyst. To accomplish this, the device must be brought to a high enough temperature to initiate propane-air catalytic reactions. This ignition temperature is significantly higher than that required for the hydrogen-air mixture and is on the order of 600 K [20]. This temperature was not attainable with the external heater. However the heater can be used to

ignite a hydrogen-air mixture that can further heat the catalyst to the required level for propane mixtures. Propane is then added in small quantities until its ignition is observed via an additional temperature rise. At this point, the hydrogen concentration is lowered while propane is added to the mixture until there is only propane and air. More details of the ignition procedure and conversion to propane-air operation are contained in reference [9].

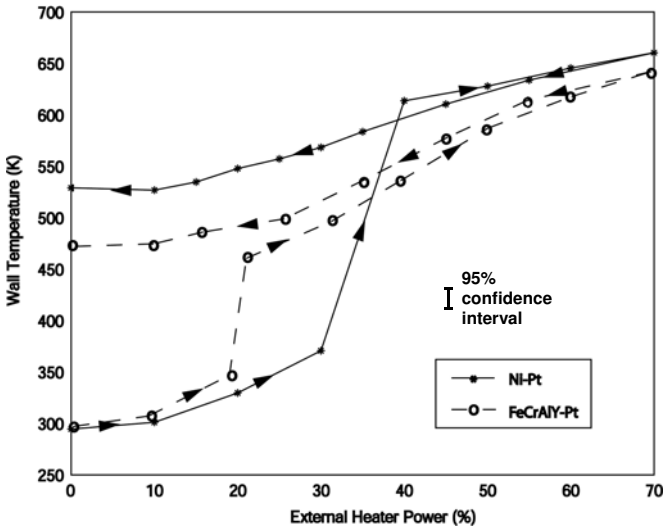

Figure 9. Ignition characteristics for catalytic microcombustors.

4.2 PERFORMANCE TESTING

Initial tests were performed on combustors which were fabricated without platinum on the substrate surface. This was done to isolate the effect of the foam structure itself inside the combustion chamber. Figure 10 shows the exit gas temperature for such a device with uncoated nickel foam material operating with propane-air combustion. The temperatures and flow rates are comparable to that reported in [3,5,9] for gas-phase devices and indicates that there is no catalytic activity and minimal effect from the foam itself.

In the case of the microcombustors with platinum catalyst coatings, significant performance improvement was achieved. Figures 11 and 12 show exit gas temperatures and overall combustor efficiency comparisons for the nickel foam (95% porous) and FeCrAlY foam (88.5% porous) devices both operating at a stoichiometric equivalence ratio. The lower porosity FeCrAlY combustor achieved exit gas temperatures over 150 K higher than the devices with the nickel substrate. This corresponds to an approximately 2%-10% higher efficiency over a range of mass flow rates. The sharp drop in performance at 0.35 g/s was a result of transients from the mass flow controllers that were operating at maximum flow levels. Although these temperatures and efficiencies are low, the mass flow rates achieved were in excess of 0.35 g/s, which satisfies the design mass flow rate for the microengine and exceeds that required for a lower flow rate engine design. These mass flow rates of interest are noted on the figures with vertical dashed lines. The maximum power density achieved for the platinum on nickel device was approximately 1050 MW/m^3, which is a 7.5-fold increase over gas-phase propane-air power densities and about 95% of that for gas-phase hydrogen-air mixtures. For the less porous platinum on FeCrAlY combustor, the maximum power density was 1200 MW/m^3, which is approximately an 8.5-fold increase over gas-phase propane-air operation and about a 10% increase over that achieved by the gas-phase hydrogen-air device.

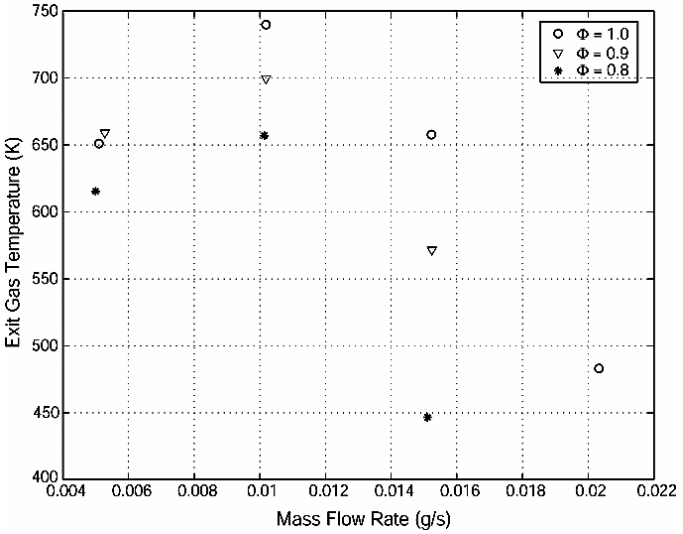

Figure 10. Exit gas temperature for microcombustor with non-catalytic foam.

The overall combustor efficiency can be broken down into its thermal and chemical components. Wall temperature measurements combined with a 1-D heat transfer model [3] reveal that although heat loss is greater than in the gas-phase case, losses are dominated by chemical inefficiency. Figure 13 shows a breakdown of the efficiencies in the nickel-platinum device for a stoichiometric mixture ratio. The chemical efficiency at the mass flow rates of interest was approximately 30%. Similar trends were observed in the FeCrAlY device although chemical efficiency was approximately 40% between mass flow rates of 0.15-0.30 g/s.

Pressure drop through the combustor is also a critical parameter for the overall engine design. Due to thermodynamic cycle constraints for engine operation, total pressure loss must be limited to less than 5%. The pressure losses from the two devices are compared in Figure 14 for operation at an equivalence ratio of unity. The lower porosity (higher density) FeCrAlY material exhibits higher pressure loss as expected. However, both devices are below the 5% total pressure loss constraint at mass flow rates of interest.

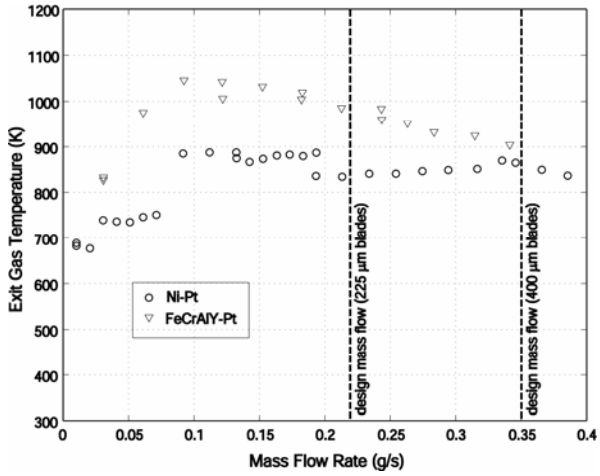

Figure 11. Exit gas temperature plot comparing Ni-Pt and FeCrAlY-Pt devices for ϕ=1.

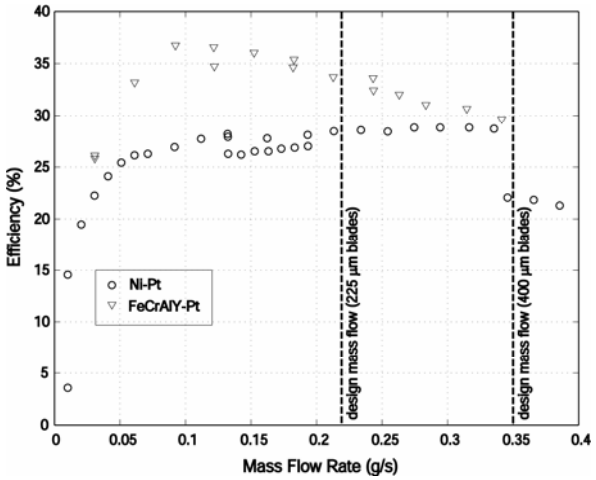

Figure 12. Overall combustor efficiency plot comparing Ni-Pt and FeCrAlY-Pt devices for ϕ=1.

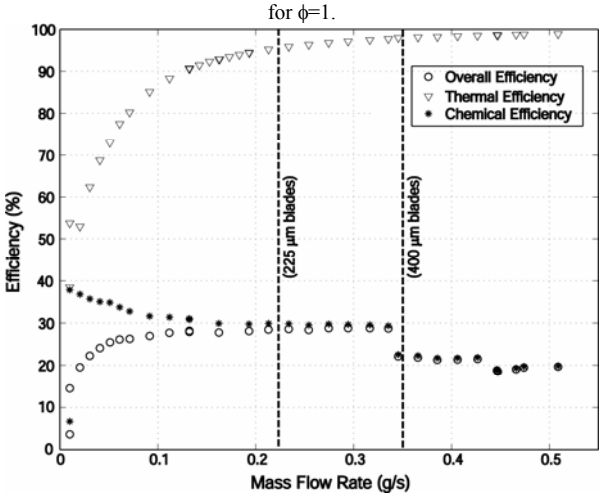

Figure 13. Efficiency breakdown for catalytic microcombustor with Ni-Pt, ϕ=1.0.

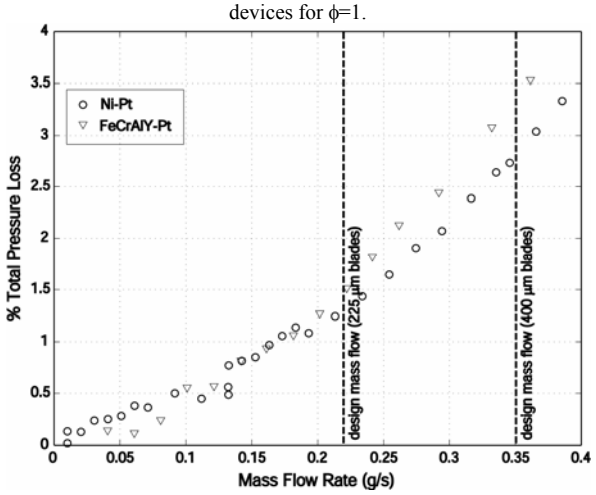

Figure 14. Total pressure loss plot comparing Ni-Pt and FeCrAlY devices for ϕ=1.

4.3 FAILURE MECHANISMS

Testing of microcombustors with 78% porous Inconel-625 foam was not successful. Three devices were packaged and tested. None of these combustors would ignite with hydrogen-air or propane-air mixtures. The typical ignition procedures were attempted followed by higher heater settings and various flow rates and equivalence ratios. None of these variations on the startup procedure were successful. The inability to light these combustors may have been due to the fuel-air mixture channeling around the foam rather than through it. Significant gaps may have been present around the foam due to the need to ensure that it easily fit into the combustion chamber for fabrication purposes. Other possible failure mechanisms include platinum agglomeration during high temperature processing and inadequate platinum coverage inside the foam.

The nickel-platinum devices exhibited sporadic performance as well. Several devices ignited and operated only at lower temperatures. This was likely a result of platinum diffusion into the nickel substrate material. This was confirmed by a materials characterization analysis which is summarized in reference [9]. As a result, the FeCrAlY-platinum devices were fabricated with a ceramic diffusion barrier layer. This prevented inter-diffusion of the two metals during the high temperature processing steps, but later led to some reduction of active surface area via agglomeration of the platinum layer [9,12].

5.0 LOW-ORDER MODELING AND ANALYSIS

Several levels of modeling have been pursued to better understand the operation of a catalytic microcombustor and to develop design recommendations. A pressure loss correlation has been utilized to estimate the drop in stagnation pressure through a given catalyst substrate. Time-scale analyses have identified the limiting factors and important non-dimensional

parameters which govern high power density catalytic combustor performance. A one-dimensional isothermal plug flow reactor model was developed to further explore combustor performance over a range of conditions and catalyst geometries. This parametric study is synthesized in model-based operating maps.

5.1 PRESSURE LOSS

Pressure loss through a porous substrate can be estimated from the Ergun equation for Reynolds numbers less than 300 (based on the thickness of a fiber or diameter of a catalyst particle) [7]:

$$-\frac{dP}{dz} = \frac{v}{l}\frac{(1-\alpha)}{\alpha^3}\left[\frac{150\mu(1-\alpha)}{l} + 1.75\rho v\right], \qquad (13)$$

where μ is the viscosity, v is velocity through the porous media, and l is a characteristic length scale, usually the width of a foam fiber or diameter of a particle in a packed bed. For the substrates of interest, Reynolds numbers are approximately 200-300.

Figure 15 shows an estimate of pressure loss through the nickel foam (95% porous) and the FeCrAlY foam (88.5% porous) used in the catalytic microcombustors. The thickness of a foam fiber was approximately 80-100 μm measured using a scanning electron microscope. The actual pressure vs. mass flow characteristic from the catalytic microcombustor experiments was used as an input. The temperature was held constant at 1000 K. The pressure drop associated with this material is low according to the Ergun calculation while the measured pressure drop in the experiment was significantly higher, in the range of 1%-3%. However, the experiment measures the loss through the entire device not just the foam. If the measured pressure loss through the device without catalyst material is subtracted from that measured in this set of experiments, the loss attributable to the foam can be estimated. Total pressure loss from the original gas-phase device can be found in reference [3]. The data points in Figure 15 are obtained by subtracting the total pressure loss of the gas-phase device from that of the catalytic microcombustor.

The additional curves shown on Figure 15 indicate the estimated pressure loss (based on equation 13) for lower porosity substrates (more dense foams). The same pressure vs. mass flow characteristic, reactor temperature, and fiber thickness was used. The stagnation pressure loss through the foam increases as porosity decreases. However, the chart indicates that a significant decrease in porosity (and increase in catalytic material) can be introduced into the reactor without violating the maximum allowable combustor pressure loss of 5%. If the 1%-3% system pressure loss is included with this estimate of catalyst pressure loss, a substrate with a porosity of approximately 80%-85% could be used in the device.

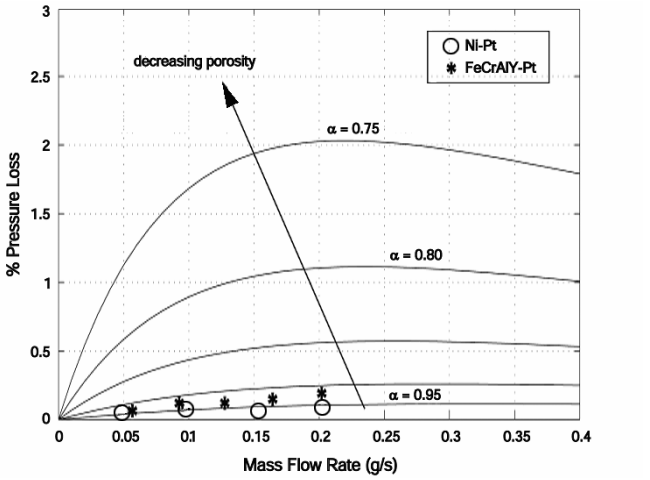

Figure 15. Pressure loss versus mass flow rate for porous media, comparing estimates from equation 7.5 and experimental data.

5.2 TIME –SCALE ANALYSIS

To determine which phenomena control the combustion process in a catalytic microcombustor, relevant physical time-scales can be evaluated. These include, reaction time, residence time, diffusion time of the fuel species, and diffusion time of the oxidizer. Residence time can be estimated from the volume, mass flow rate, pressure, and bulk gas temperature as in the gas-phase case (equation 2). Reaction rate can be obtained from an Arrhenius type rate expression. For a propane-air reaction on a platinum catalyst, the following mechanism can be used [7]

$$\left(-R_{C_3H_8}\right) = k_s\left[C_3H_8\right] \qquad (14)$$

where the rate constant is

$$k_S = 2.4\times10^5 \exp\left(\frac{-1.08\times10^4}{T}\right). \qquad (15)$$

The reaction rate has units of mol/m^{2}s where the area is the catalyst surface area. Molecular diffusion coefficients for propane and oxygen diffusion through air can be obtained from the Fuller correlation (equation 5) [7].

Using estimates of these various time-scales, non-dimensional parameters can be calculated and used to determine the governing physical phenomena. These parameters and their approximate values for a catalytic microcombustor are summarized below in Table 2. From this simple time-scale analysis, it is clear that diffusion of reactants to the surface is a controlling parameter. The diffusion-based Damköhler number indicates that the surface reaction rate is much faster than the rate of diffusion to the surface. The Peclet

number indicates that reactants can flow through the device without coming into contact with the active catalytic surface.

If a tubular plug flow reactor is assumed, the Peclet number can be estimated and shown to be a strong function of geometry. For a given set of flow conditions (pressure, temperature, and mass flow rate) Peclet number can be

Table 2. Summary of non-dimensional parameters.

Non-dimensional parameter	Range
$Da_1 = \frac{\tau_{residence}}{\tau_{reaction}}$	~0.5-5
$Da_2 = \frac{\tau_{diffusion}}{\tau_{reaction}}$	~30-500
$Pe = \frac{\tau_{diffusion}}{\tau_{residence}}$	~55-130

calculated for a range of diameters (or pore sizes). In this case, the gas velocity through the tube and the length of the tube are estimated based on the actual microcombustor. Figure 16 shows this parameter for P = 2 atm, T = 1000 K, and a mass flow rate = 0.3 g/s for both propane and oxygen. For the diameters (or pore sizes) of interest the Peclet number is larger than unity. It is also important to note that propane diffuses more slowly than oxygen. This results in a larger Peclet number and indicates that propane diffusion to the active surface is the governing phenomenon.

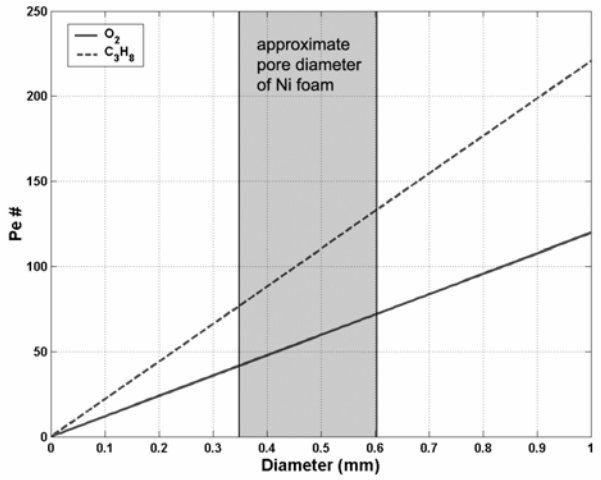

Figure 16. Peclet number versus diameter.

5.3 1-DIMENSIONAL ISOTHERMAL PLUG FLOW REACTOR MODEL

The equations developed here have been derived from a control volume analysis of a fluid element in a plug flow reactor. These equations coupled with the isothermal assumption yield trends in fuel conversion and bulk gas temperature rise through the reactor as a function of flow conditions and geometry.

The Peclet number analysis indicated that the diffusion of propane is the governing phenomenon, therefore only the mass transport and consumption of the fuel species is taken into account in all subsequent derivations. Homogeneous gas-phase reactions will be neglected and the catalytic reaction mechanism shown in equations 14 and 15 will be utilized for all further analyses.

A steady-state gas-phase mole balance across the control volume results in

$$C_b v \frac{dY_{f,b}}{dz} + a_v k_m C_b \left(Y_{f,b} - Y_{f,S}\right) = 0 \cdot \tag{16}$$

The surface area-to-volume ratio can be written in terms of porosity and foam fiber thickness as

$$a_v = \frac{4(1-\alpha)}{w} \cdot \tag{17}$$

A mole balance performed at the catalyst surface yields

$$k_m C_b \left(Y_{f,b} - Y_{f,S}\right) = \left(-R_f\right)_S (1-\alpha) \tag{18}$$

while an energy balance across the fluid element provides the final equation.

$$-\rho C_p v \frac{dT_b}{dz} + a_v h\left(T_S - T_b\right) = 0 \tag{19}$$

Analytical solutions to these equations can be found or an appropriate numerical method can be applied to solve the system.

Correlations for gases in packed bed reactors have been used to approximate the heat and mass transfer coefficients in porous substrates. These transport coefficients are given in terms of non-dimensional j factors; j_D for mass transfer and j_H for heat transfer.

$$j_D = \frac{k_m}{v} Sc^{2/3} \tag{20}$$

$$j_H = \frac{h}{C_p \rho v} Pr^{2/3} \tag{21}$$

These j factors can be estimated using the following correlations [7].

$$j_D = j_H = 0.91 Re_j^{-0.51} S_f \qquad Re_j < 50 \tag{22}$$

$$j_D = j_H = 0.91 Re_j^{-0.41} S_f \qquad Re_j > 50 \qquad (23)$$

S_f is the shape factor and for this analysis a value of 0.79 was used (shape factor for ring-type structures). The Reynolds number used here can be found from

$$Re = \frac{\rho v w}{6(1-\alpha)\mu S_f}. \qquad (24)$$

The boundary conditions required to run the model include the inlet bulk gas temperature, the inlet bulk gas fuel mole fraction (obtained from equivalence ratio), and the inlet surface mole fraction. The catalyst surface temperature also must be specified and due to the isothermal condition is constant throughout the reactor. A typical set of boundary and flow conditions is shown in Table 3.

Table 3. Typical boundary and flow conditions for reactor inlet in 1-D isothermal plug flow model.

PARAMETER	VALUE
T_b	500 K
T_S	1000 K
$Y_{fuel,b}$ (from ϕ)	0.04 (ϕ=1.0)
$Y_{fuel,S}$	0.00
Pressure	2 atm
Mass flow	0.3 g/s

Figures 17 and 18 show temperature and fuel concentration profiles respectively. The conditions listed above in Table 3 were used to generate these results along with a substrate porosity of 95% and an average foam fiber thickness of 90 μm.

Figure 19 shows a comparison of the model results to that obtained in the experiments for both the 95% and 88.5% porous substrates. Fuel conversion is the parameter being compared. The approximate geometries of the substrate materials were used as well as the measured pressure and mass flow rates from the experiment. The model replicates the trends shown in the experiments. These trends include a relatively constant fuel conversion over a broad mass flow range and the lower porosity material resulting in higher conversions and exit gas temperatures. However, the model does not predict overall levels well. Likely reasons for this are variations in the substrate geometry and the platinum coverage as well as flow leakage around the foam material.

A model sensitivity study was performed and indicated that a variation of 20% in surface area-to-volume ratio would result in an approximately a 10% change in fuel conversion. The sensitivity to leakage flow around the foam material can also be estimated. The conversion for a reduced flow rate can be mass averaged with an unreacted leakage flow to simulate this scenario. Results indicate that fuel conversion changes by approximately 7% with each 20% increment in leakage. Leakages around the catalyst are expected to be ~20% however an actual measurement is not possible.

With this model, the effect of key design variables such as porosity and surface area can be further examined. For constant flow conditions, the model can produce fuel conversion profiles for various porosity and surface area materials. Figure 20 shows trends in fuel conversion for increasing surface area-to-volume ratios using the conditions listed in Table 3. The profiles indicate that higher surface area-to-volume ratios (usually a result of lower porosity for a constant fiber thickness) will significantly improve fuel conversion.

The 1-D isothermal plug flow model can also be used to visualize a catalytic microcombustor's operating space. Figure 21 shows lines of constant power density on a plot of total pressure loss through the device versus catalyst temperature for an equivalence ratio of unity. The total pressure loss is estimated by adding the pressure loss through the substrate material as predicted by the Ergun equation to an estimate of the pressure loss due to the silicon structure [3]. The maximum power density is obtained from the exit gas temperature predicted by the model. Figure 21 indicates that at higher pressure loss (higher surface area-to-volume ratio) and higher catalyst temperatures, combustor performance improves. It is also clear that by relaxing the pressure loss constraint and utilizing a catalyst which can survive at higher temperatures, the available operating space will broaden. The current microengine constraint of less than 5% total pressure loss is indicated by the black line and gray shaded area. The shaded area above a 1400 K catalyst temperature represents an approximate failure temperature for the catalyst layer.

The catalytic microcombustor operating space can be viewed more generally by plotting non-dimensional parameters. Figure 22 shows lines of constant combustor efficiency on a chart with Peclet number versus thermal efficiency. As Peclet number decreases, combustor efficiency increases due to the time available for diffusion of the reactant species to the active surface. However, as heat is lost from the system (lower thermal efficiency), the overall efficiency decreases.

6.0 DESIGN RECOMMENDATIONS

Design recommendations for catalytic microcombustion systems are listed below. These recommendations are based on the experimental results presented in Section 4, the low-order modeling in Section 5, and a materials characterization study described in references [9].

1. High power density catalytic microcombustors are diffusion controlled. A designer should seek to approach the high temperature reaction controlled regime to maximize performance. This can be achieved by implementing the following:

a. Utilize the most thermally durable catalytic materials to achieve high temperature operation.
b. Utilize the highest surface area-to-volume ratio substrate material available which does not violate the system pressure loss constraint.
c. Relax the total pressure loss constraint as far as the thermodynamic cycle will permit.

2. Searching for a more active catalytic material is not required unless:
   a. The ignition transient is of concern.
   b. The overall design lies in the reaction-controlled regime.
3. Although thermal management was not a problem in the devices tested here due to poor thermal contact of the catalyst to the silicon, leakage paths around the catalyst material, and the recirculation jacket, a more intimately contacted catalyst material operating at higher temperatures will likely suffer from significant thermal losses. A materials solution such as a thermal barrier combined with a concept similar to the recirculation jacket may mitigate these losses.
4. Due to high temperature processing and operation, substrate materials for noble metal catalysts should be resistant to solid diffusion or include a diffusion barrier layer.
5. Catalytic materials which are less likely to agglomerate at high temperatures should be used.
6. A robust fabrication and assembly process which does not result in leakage paths around the catalyst material should be considered when designing the device.

7.0 SUMMARY AND FUTURE WORK

Due to the poor performance of gas-phase microcombustors with hydrocarbon fuels, a strategy of heterogeneous surface catalysis has been pursued. This offered the potential to increase hydrocarbon microcombustor power density by directly increasing reaction rates. A catalytic six-wafer device compatible with the microengine geometry was developed.

This combustor consisted of filling the combustion chamber with a foam material coated with platinum as the active catalytic surface. Several catalyst substrate materials

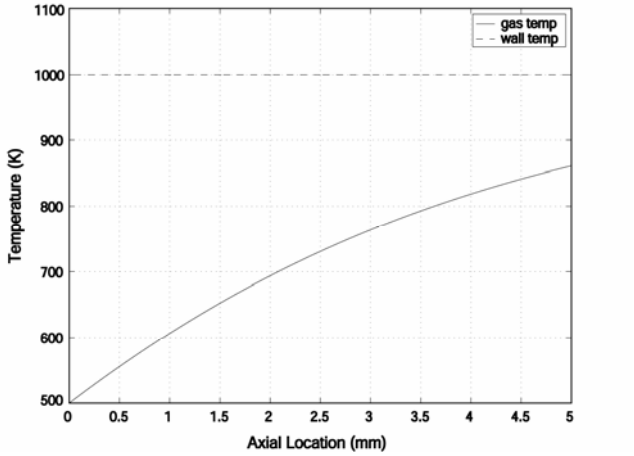

Figure 17. Axial temperature profile in porous media plug flow reactor.

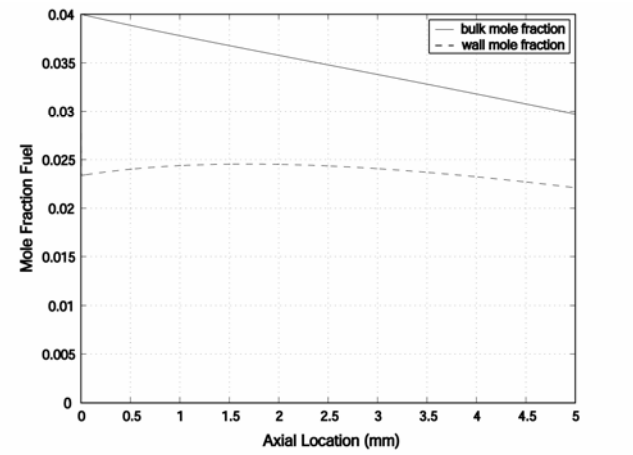

Figure 18. Axial fuel concentration profile in porous media plug flow reactor.

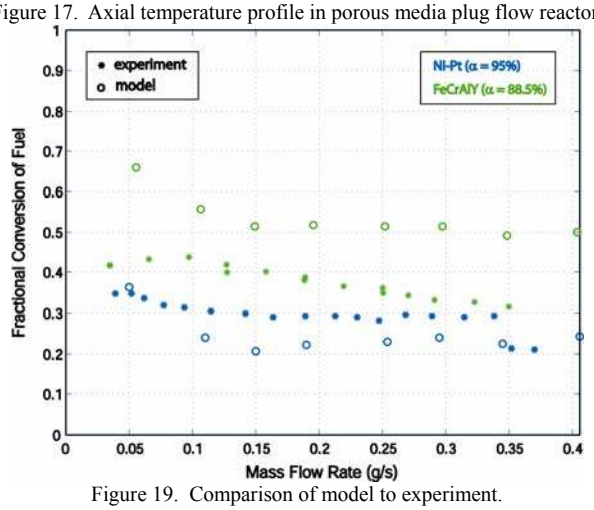

Figure 19. Comparison of model to experiment.

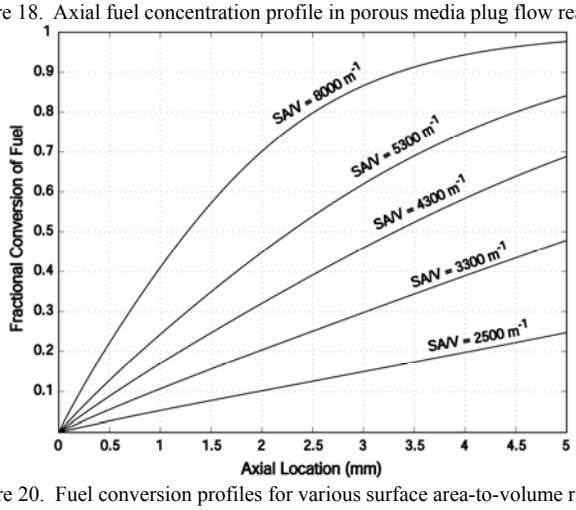

Figure 20. Fuel conversion profiles for various surface area-to-volume ratios.

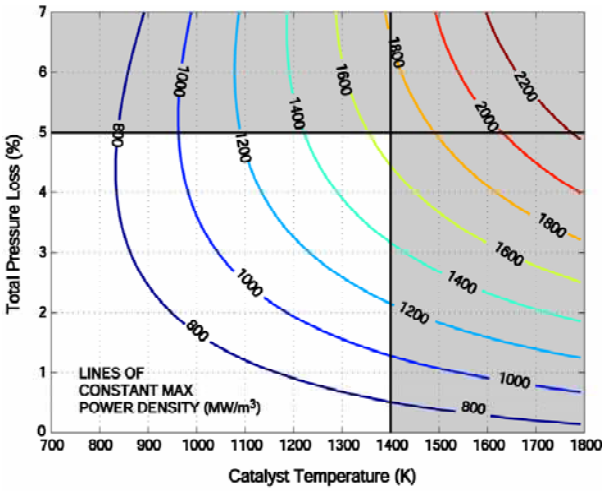

Figure 21. Operating space for catalytic microcombustor; lines of constant power density.

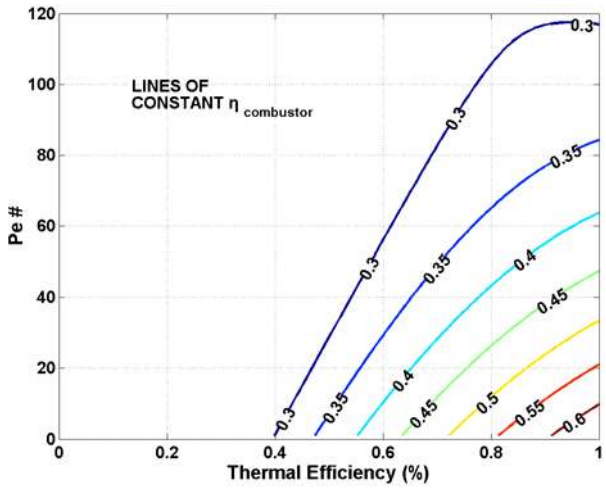

Figure 22. Non-dimensional operating space; Peclet number versus thermal efficiency.

with varying porosity and surface area were tested. The combustors were ignited via preheating of the entire chip and flowing a hydrogen-air mixture through the device. After catalytic ignition of the hydrogen-air mixture, operation was converted to propane-air autothermal combustion.

The 95% porous foam devices achieved exit gas temperatures in excess of 850 K and efficiencies of approximately 30% with propane. Although the efficiency and gas temperatures were low, this combustor operated at high mass flow rates compared to previous gas-phase combustors. Mass flow rates over 0.35 g/s were achieved and power density was a 7.5-fold increase over propane-air gas-phase operation. The devices with 88.5% porous FeCrAlY foam achieved exit gas temperatures approaching 1100 K and efficiencies near 40%. The power density of this device was an 8.5-fold increase over the comparable gas-phase microcombustor.

Low-order modeling including a pressure loss correlation, time-scale analyses, and a 1-D isothermal plug flow reactor model indicated that high power density operation is diffusion controlled and the relatively lower porosity and higher surface area-to-volume ratio of the FeCrAlY foam substrate was responsible for improved performance.

Based on the results of this work, future research may include the following:

Improved Ignition Schemes

Although the ignition procedure described in Sections 4.1 was effective for these bench-top catalytic microcombustor experiments, a more robust and self-contained system would be optimal for a practical device. A simple and effective means of achieving catalytic ignition of hydrocarbons over noble metal catalysts is to resistively heat the catalyst material itself [20,21]. By bringing the catalyst temperature up to the ignition temperature required for propane-air mixtures, the external preheating and hydrogen ignition procedure could be eliminated. In order to accomplish this in a device like the six-wafer microcombustors presented here, there would need to be significant fabrication changes. This would involve incorporating multi-level electrical interconnects into the device and contacting them to the metal catalyst material. These interconnects would extend to the chip's surface where they could be connected to a power source for the resistive heating.

Hybrid Microcombustors

The catalytic microcombustors were successful in significantly increasing power density and mass flow range for hydrocarbon–fueled devices. However, the exit gas temperatures achieved were significantly lower than that required for the microengine thermodynamic cycle. Attaining these temperatures in a catalytic device of this kind is unlikely because the catalyst wall temperatures required would be high enough to cause significant agglomeration of the catalyst layer. In addition, to accomplish this in a relatively small volume the total pressure loss would be significantly greater than the 5% constraint imposed by the engine cycle. Although the gas-phase devices were capable of achieving high exit gas temperatures and efficiencies with hydrogen-air mixtures, their mass flow rate capability was significantly less than the engine design flow rate of 0.35 g/s and was even worse with hydrocarbon fuels.

As a result, a strategy for achieving both high temperature and high mass flow rate operation in a minimum volume may be to combine the two devices into a hybrid microcombustor similar to that proposed and developed by Dalla Betta *et. al.* for large-scale, low NO_X applications [22,23].

For this type of device, the entrance region of the combustion chamber would consist of a porous substrate or micro-channel type geometry coated with a catalyst layer. The first stage would ignite the fuel-air mixture and bring it to some mid-range temperature (~1000 K) with minimal total

pressure loss. A second stage of open volume for homogeneous combustion would follow. The exit conditions of the catalytic section would serve as the inlet to the gas-phase section, which would burn the remaining fuel-air mixture. The combustion in the second stage would proceed quickly due to the already high inlet gas temperature ultimately achieving the 1600 K exit gas temperature in a minimum total volume.

Liquid Fuels

One final subject of potential future work is to include the use of liquid fuels such as kerosene and JP8 in microcombustor development. These types of fuels are the most commonly used logistics fuels. The catalytic microcombustors described in this paper may be a first step toward achieving high power density operation with logistics fuels.

The use of these liquid fuels constitutes a significant development challenge. Some development issues may include:

1. Liquid fuel injection and droplet atomization.
2. Condensation of the fuel upstream of the combustion chamber.
3. Evaporation of droplets and fuel-air mixing after atomization.
4. Diffusion of the larger hydrocarbon molecules to a catalyst surface.
5. Ignition procedures/methods.
6. Reaction rates of heavy hydrocarbons on catalysts.
7. Coking/fouling of catalyst surface.

8.0 ACKNOWLEDGMENTS

This work was conducted as part of the MIT Microengine Project and the authors are grateful to Professor A. Epstein for his leadership of this program. The entire Microengine team, especially N. Miki, L. Ho, and X. Zhang, should also be acknowledged. The support of the technical and administrative staff at the MIT Gas Turbine Laboratory, particulary V. Dubrowski, J. Costa, J. LeTendre, S. Parker, J. Finn, M. McDavvitt, and L. Martinez, is greatly appreciated. V. Sciortino and J. Peterson at Ionic Fusion Corporation are thanked for their innovative film deposition technique, G. Simpson at Vetrofuse Inc. and Mike Anzalone at Thunderline-Z Inc. for assistance in packaging. This work has been supported by the US Army Research Laboratory under the Collaborative Technology Alliance agreement number DAAD19-01-2-0010.

REFERENCES

[1] Epstein *et al*., "Micro-Heat Engines, Gas Turbines, and Rocket Engines", presented at the 28th AIAA Fluid Dynamics Conference, 1997.

[2] Groshenry, C., "Preliminary Study of a Micro-Gas Turbine Engine", S.M. Thesis, Massachusetts Institute of Technology, 1995.

[3] Mehra, A., "Development of a High Power Density Combustion System for a Silicon Micro Gas Turbine Engine", Ph.D. Thesis, Massachusetts Institute of Technology, 2000.

[4] Mehra *et al*., "A 6-Wafer Combustion System for a Silicon Micro Gas Turbine Engine", *IEEE/ASME Journal of Microelectromechanical Systems*, 2000.

[5] Spadaccini *et al.*, "High Power Density Silicon Combustion Systems for Micro Gas Turbine Engines," *ASME Journal of Engineering for Gas Turbine and Power*, Vol. 125, pp. 709-719, July, 2003.

[6] Waitz *et al*., "Combustors for Micro Gas Turbine Engines", *ASME Journal of Fluids Engineering*, Vol. 20, pp. 109-117, March 1998.

[7] Hayes, R.E., and Kolaczkowski, S.T., Introduction to Catalytic Combustion, Gordon and Breach Science Publishers, Canada, 1997.

[8] Mehra *et al*., "Development of a Hydrogen Combustor for a Microfabricated Gas Turbine Engine", presented at the Solid-State Sensor and Actuator Workshop at Hilton Head, 1998.

[9] Spadaccini, C.M., "Combustion Systems for Power-MEMS Applications," Ph.D. Thesis, Massachusetts Institute of Technology, Department of Aeronautics and Astronautics, 2004.

[10] Fernandez-Pello *et al.*, "MEMS Rotary Engine Power System," Power MEMS 2002: International Workshop on Power MEMS, Technical Digest, pp. 28-31, Tsukuba, Japan, November, 2002.

[11] Arana, L.R., "High-Temperature Microfluidic Systems for Thermally-Efficient Fuel Processing," Ph.D. Thesis, Massachusetts Institute of Technology, Department of Chemical Engineering, 2003.

[12] Schaevitz, S.B., "A MEMS Thermoelectric Generator," S.M. Thesis, Massachusetts Institute of Technology, Department of Electrical Engineering and Computer Science, 2000.

[13] Maruta *et al.*, "Catalytic Combustion in Microchannels for MEMS Power Generation," The Third Asia-Pacific Conference on Combustion, Seoul, Korea, June 2001.

[14] Hatfield, J.M., and Peterson, R.B., "A Catalytically Sustained Microcombustor Burning Propane," 2001 IMECE, New York, NY, November, 2001.

[15] Spadaccini *et al.*, "Preliminary Development of a Hydrocarbon-Fueled Catalytic Micro-combustor," *Sensors and Actuators A: Physical*, Vol. 103, pp. 219-224, 2003.

[16] Ionic Fusion Corporation, corporate literature, Longmont, CO, 2003.

[17] Harrison, T., "Packaging of the MIT Microengine", S.M. Thesis, Massachusetts Institute of Technology, 2000.

[18] London, A.P., "Development and Test of a Microfabricated Bipropellant Rocket Engine," Ph.D. Thesis,

Massachusetts Institute of Technology, Department of Aeronautics and Astronautics, 2000.
[19] Peck, J., "Development of a Catalytic Combustion System for the MIT Micro Gas Turbine Engine," S.M. Thesis, Massachusetts Institute of Technology, Department of Aeronautics and Astronautics, 2003.
[20] Williams *et al.*, "Bifurcation Behavior in Homogeneous-Heterogeneous Combustion: I. Experimental Results Over Platinum," *Combustion and Flame*, Vol. 84, pp 277-291, 1991.
[21] Goralski, Jr., C.T., and Schmidt, L.D., "Lean Catalytic Combustion of Alkanes at Short Contact Times," *Catalysis Letters*, Vol. 42, pp. 15-20, 1996.
[22] Dalla Betta *et al.*, "Catalytic Combustion Technology to Achieve Ultra Low NO_x Emissions: Catalyst Design and Performance Characteristics," *Catalysis Today*, Vol. 26, pp. 329-335, 1995.
[23] Dalla Betta *et al.*, "Application of Catalytic Combustion Technology to Indutrial Gas Turbines for Ultra-Low NO_x Emissions," ASME International Gas Turbine and Aeroengine Congress and Exposition, paper # 95-GT-65, Houston, TX, June, 1995.